Design and Fabrication of a Functional Fiber for Micro Flow Sensing

Tingting Yuan, Xiaotong Zhang, Qi Xia, Yiping Wang, and Libo Yuan

***Abstract*—We designed a novel dual-core fiber with a large side air hole near the center core, which microstructure optical fiber can integrate with microchannel and interferometer in a single fiber. To fabricate this special optical fiber, first, we drill a small hole in the side of a standard single-core fiber preform, insert a thin-clad core preform into the small hole, and then heat and fuse together. Finally, we drilled a larger hole near the center core. In the process of drawing the fiber, the large hole should be filled with nitrogen at a constant pressure to prevent the hole from collapsing. The air hole of the special optical fiber can be used as a channel for microfluidic transmission, and the air hole is in close contact with the central core and away from the eccentric core, so this microstructure optical fiber is very suitable for use as a compact in-fiber integrated microfluidic sensors.**

***Index Terms*—Dual-core optical fiber, microchannel fiber, microfluidic transmission.**

I. Introduction

In recent years, new structures and new materials of optical fiber are emerging continuously, which provide a variety of possibilities for the expansion of new functions of optical fiber. Such as photonic crystal fiber[1], [2], multicore fiber[3]–[5], chiral fiber[6]–[8] and metamaterial fiber[9], [10]. The appearance of these optical fibers provides new vitality for the development and application of optical fiber technology. A large number of new properties (infinite cut-off single-mode, anomalous dispersion, high nonlinearity, etc.) are brought to optical fiber devices through microstructures. In addition, it also provides a flexible new platform for interdisciplinary applications based on the interaction of light-matter, light-sound, and light-mechanical. The new microstructured optical fibers and devices have been widely used in the fields of optical transmission, optical sensing, spectroscopy, nonlinear optics and quantum optics. It is opened the new research directions of lab-in/on-fiber [11], [12].

Hollow photonic crystal fiber was invented by P. Russell using a bandgap waveguide mechanism [13], [14]. This kind of fiber can greatly improve the interaction between light and microfluidic material. However, due to the strict requirements of the bandgap structure, the preparation of photonic crystal fiber is difficult. In addition, because of the porous bandgap of the microstructure of the cladding, when the microflow is injected into the central air hole of the fiber, the liquid easily penetrates into the microstructure cladding, so it is difficult to apply. In 2000, C. E. Kerbage et al. proposed a six-hole fiber [15], which has a highly doped core and a low refractive index cladding and six large air holes surrounding the central core. Different air hole can be filled with materials with different characteristics to prepare different optical fiber devices, so this kind of optical fiber can be used for microflow measurement. But, on the one hand, the interaction between light and matter is weakened due to the large distance between the fiber core and the microflow in the hole. On the other hand, because the fiber has only one core, it is difficult to construct a double-path interferometer on the same fiber.

In order to solve the problem of efficient interaction between light and material and integrating the interferometer optical path into the same optical fiber, a new type of microstructure optical fiber with dual optical waveguide and material microchannel composite integration is presented. By optimizing the geometric parameters and refractive index of the optical fiber, a specially designed optical fiber can be provided to realize the function of the integrated optical fiber device.

II. Design and Fabrication of the Fiber Preform

The material in the hole will strongly interact with the central core but has no effect on the eccentric core. Fig. 1(a) illustrates the schematic diagram of an optical fiber with an air hole and two cores designed and manufactured by us. The size of the eccentric core is the same as the size of the central core. The air hole is very close to the center core, so this new type of optical fiber is very suitable for microfluidic optical sensing. The sensor has a microchannel that runs through the entire device, which the solution can flow. The sensor has two optical paths, where the

Manuscript received June 23, 2020; revised August 12, 2020; accepted September 1, 2020. Date of publication September 11, 2020; date of current version January 2, 2021. This work was supported in part by The National Key Research and Development Program of China under Grant 2019YFB2203903, in part by the National Natural Science Foundation of China under Grant 61905154, Grant 61535004, Grant 61827819, and Grant 61735009, in part by the China Postdoctoral Science Foundation funded project under Grant 2019M663051, partially supported by the special fund for Guangxi Bagui scholars, and in part by Guangxi Project (AA18242043, AD17195074) *(Corresponding author: Libo Yuan.)*

Tingting Yuan and Yiping Wang are with the Key Laboratory of Optoelectronic Devices and Systems of Ministry of Education, College of Optoelectronic Engineering, Shenzhen University, Shenzhen 518060, China (e-mail: ttyuan90@foxmail.com; ypwang@szu.edu.cn).

Xiaotong Zhang and Qi Xia are with the Key Laboratory of In-Fiber Integrated Optics, Ministry Education of China, Harbin Engineering University, Harbin 150001, China (e-mail: zhangxiaotong1211@foxmail.com; xiaqi_hrb@163.com).

Libo Yuan is with the Photonics Research Center, School of Electronic Engineering and Automation, Guilin University of Electronic Technology, Guilin 541004, China (e-mail: lbyuan@vip.sina.com).

Color versions of one or more of the figures in this article are available online at https://ieeexplore.ieee.org.

Digital Object Identifier 10.1109/JLT.2020.3022108

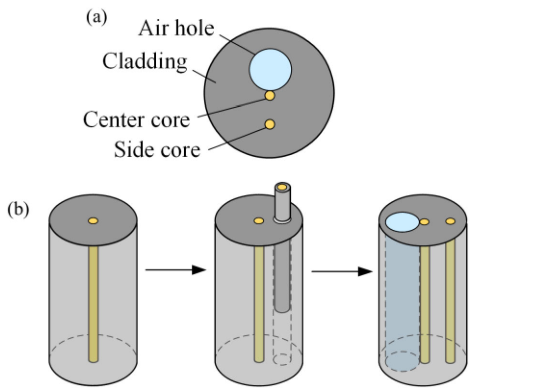

Fig. 1. (a) The schematic diagram of the dual-core optical fiber with a side-hole; (b) Fabrication process of the dual-core fiber preform with a large hole: first, a single core fiber preform; second, dual-core preform; and third drill an air hole in the dual-core preform.

center core near the hole is used as the measurement path, and the eccentric core away from the hole is used as the reference path. The material in the hole will strongly interact with the central core but has no effect on the eccentric core.

The proposed optical fiber preform is different from the traditional single-core optical fiber preform (Fig. 1b). First, we use the normal modified chemical vapor deposition (MCVD) technology to fabricate standard single-core fiber preforms. Then, a small hole is drilled in the single-core fiber preform, and the core preform with a thin cladding is inserted into the drilled hole of the fiber preform. In order to insert the core rod into the hole, the diameter of the core preform is slightly smaller than the diameter of the drill hole. Subsequently, the combined preforms were heated until melted, and then the preforms were sintered twice in a vacuum to exclude air in the hole. Finally, we drilled a larger hole in the preform near the center core and away from the side core. A dual-core optical fiber preform with a large hole was obtained.

III. Drawing the Fiber With Dual-Core and a Side-Hole

For preparing microstructured fibers similar to conventional fibers, the first is to prepare a preform. When the preform is ready, it will be heated at a high temperature in a drawing furnace. When the preform melts and flows, a drop of the preform is pulled from the bottom of the furnace, passes the coating system, and then enters the roller mechanism. The roller will wind the fiber at a constant speed to ensure the constant diameter of the fiber, and the fiber will be measured by parameters monitor. Finally, a dual-core optical fiber with an air hole can be easily manufactured up to a kilometer in length. The drawing process is shown in Fig. 2(a). Due to the high temperature, we need to add a stable nitrogen pressure to balance the pressure inside and outside the air hole to avoid collapse during stretching. Finally, the fiber is covered with a coating to protect it from mechanical damage. The fabricated optical fiber has the same strength and physical size as the standard optical fiber. The uniformity of the air hole of the fiber will have a great impact on the application of this kind of fiber. There are many parameters that will affect the consistency of the fiber air hole, therefore, we ensure the consistency of the fiber by accurately controlling parameters such as furnace temperature, drawing speed and nitrogen pressure in the air hole during the fiber drawing process. And we took photos of this fiber end faces at both ends of the 5km long fiber sample to compare the consistency of the fiber size (as shown in Fig. 2b).

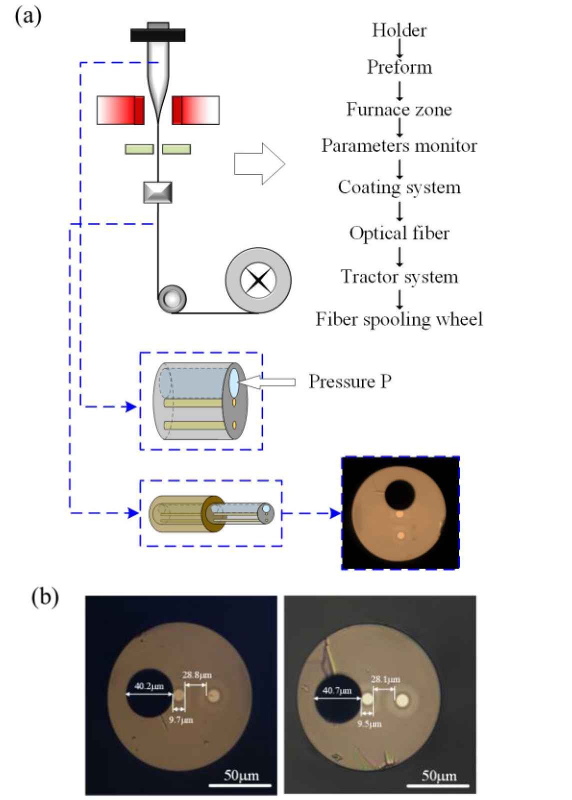

Fig. 2. (a) The drawing process of fiber with dual-core and a side-hole, insert: cross-section photograph of the fiber sample with dual-core and a side-hole. (b) Photos in fiber sample at both ends of 5 km.

The outer diameter of the fiber is 125 μm, the air hole diameter of the fiber is 40.7 μm, the distance between the two cores is 28.6 μm, a and the diameters of the central core and the eccentric core are both 9.4 μm. The cross-section view of the microstructured optical fiber captured by the CCD of the microscope is measured in Fig. 2(a) inserts. The distance between the two cores and size of the air hole have been considered. In order to ensure that the two cores will not affect each other, after calculation, the distance should be at least 20 μm. The size of the hole directly affects the speed of microflow. The smaller the hole, the greater the fluid resistance. In view of the follow-up application of the optical fiber, we will first choose larger air hole in designing.

IV. Characteristics of the Fiber With Dual-Core and a Side-Hole

A. Refractive Index Profile

As can be seen in Fig. 3, the refractive index (RI) distribution of the sample fiber measured by a refractive index profiler. The RI of the core and cladding are 1.458 and 1.4555, respectively.

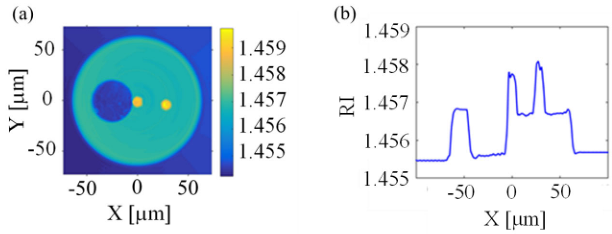

Fig. 3. RI profile of the fiber with dual-core and a side-hole. (a) RI profile of cross-section. (b) RI profile in Y = 0.

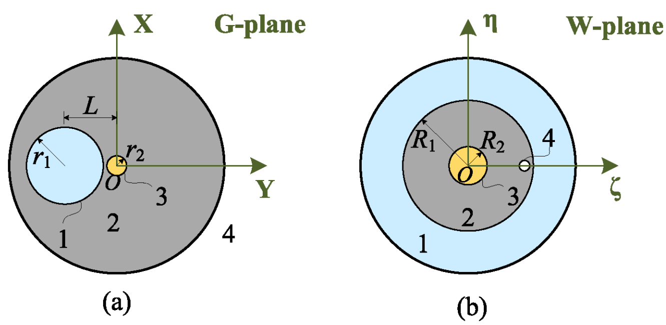

Fig. 4. The conformal transformation for the side-hole fiber. (a) Cross-section of the eccentric air hole fiber on the G-plane. (b) The concentric circles mapped on the W-plane.

Due to the special structure of this fiber, the transmission loss of the two cores is much greater than that of the traditional single-mode fiber, and the center core is adjacent to the air hole, so the loss will be greater than the side core. But the optical fiber sensor just needs a very short length, so here we do not consider the transmission loss of the optical fiber.

B. Waveguide Mode Field Characteristics of Adjacent Microflow Holes

Base on the mapping technique [16], the fiber with a side-hole could be transformed into a four layers structure from the G-plane to the W-plane, as shown in Figs. 4(a) and 4(b). In the W plan, we can get the formal solution of the Helmholtz equation in a concise way [17], on the W-plane, the Helmholtz wave equation change to the following one:

$$[\nabla^2+(k^2n^2-\beta^2)/|W'(G)|^2]\mathbf{E}=0 \tag{1}$$

Here $W'(G)=\mathrm{d}W/\mathrm{d}G$.

If the above problems can be solved, this mapping technique could be plausible. If the above problems can be solved, this mapping technique could be conceivable [18]. The transformation relationship between the G-plane to the W-plane can describe as

$$W(G)=-s\frac{z-t}{z-s}(L>0,s<t<0) \tag{2}$$

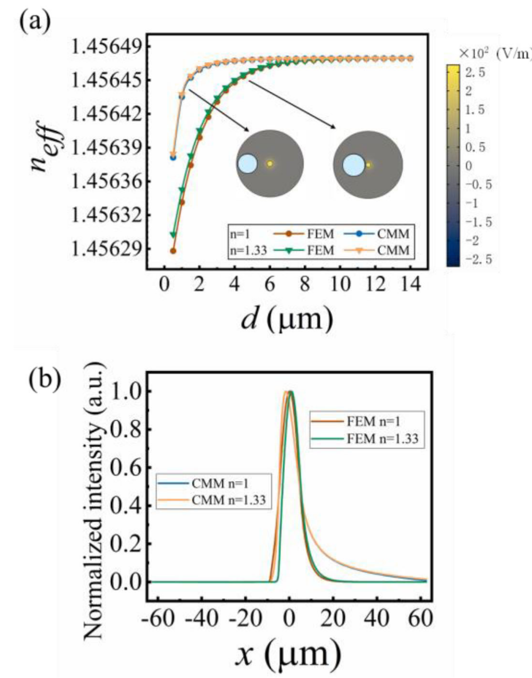

Fig. 5. The difference between FEM and CMM. (a) Effective RI of an eccentric air hole optical fiber. (b) The electric field mode distribution in the same Cartesian coordinate system, respectively in air and water.

In Eq. (2), *s* and *t* are the roots of the following equations

$$\begin{cases} st=r_2^2 \\ (s+L)(t+L)=r_1^2 \end{cases} \tag{3}$$

R_2 and R_1 are radiuses of inner and outer circles respectively in the W-plane. Assuming $R_1=r_1$, Eq. (2) can be rewritten as

$$z=\frac{Ws+st}{W+s} \tag{4}$$

If $W=r\exp(j\varphi)$, we obtain

$$1/|W'(z)|=\left|\frac{1-t/s}{1+2r\exp(j\varphi)/s+r^2/s^2}\right| \tag{5}$$

From Eq. (5), $1/|W'(G)|^2$ can expand into a series of power *r/s*:

$$1/|W'(G)|^2=\left(1-\frac{t}{s}\right)^2\Big/\left(1+\frac{4r\cos\varphi}{s}+\cdots\right) \tag{6}$$

If $L+s$ is great enough, the term $4r\cos\varphi/(L+s)$ can be absolutely negligible (<1%) [19]. Thus, the zero-order approximation of Eq. (1) can be expressed as follow:

$$\left[\nabla^2+\left(1-\frac{t}{s}\right)^2(k^2n^2-\beta^2)\right]\mathbf{E}=0 \tag{7}$$

Based on Eq. (7), the longitudinal field components can be written as

Here J_m is mth order Bessel function of the first kind, I_m and K_m are mth order modified Bessel functions of the first and

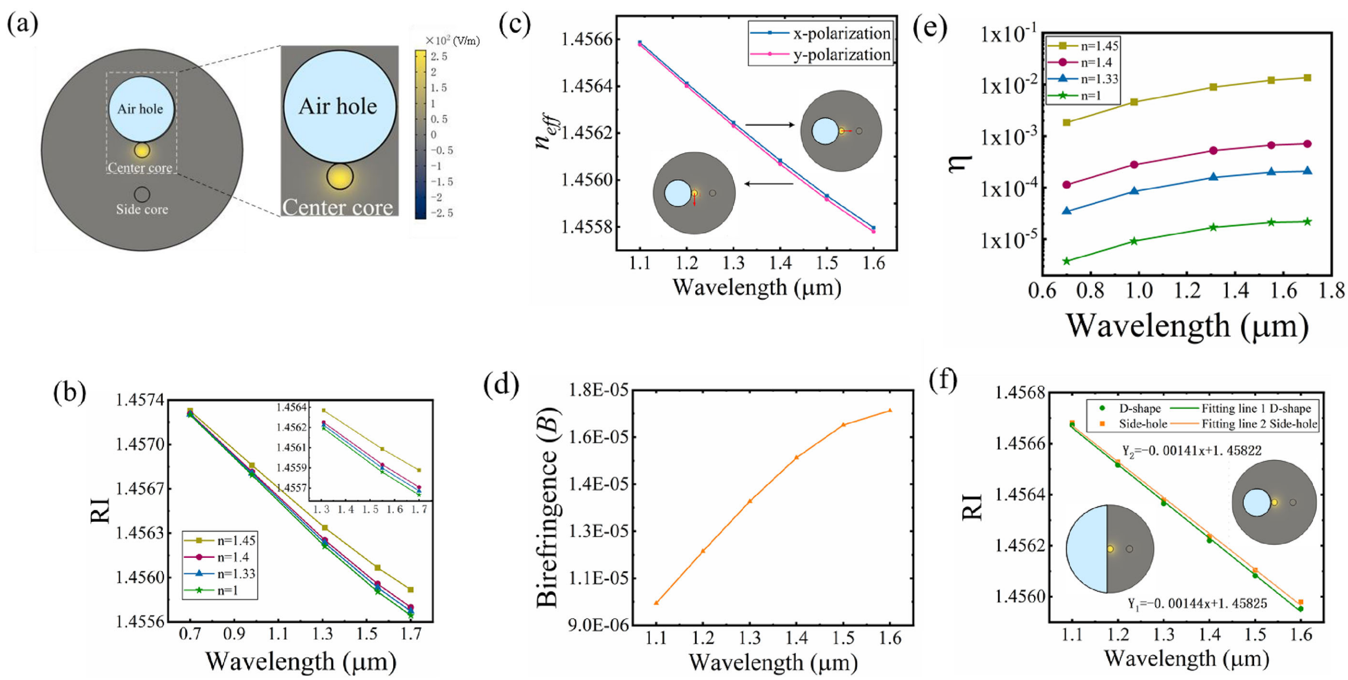

Fig. 6. (a) Simulation results of evanescent field distribution with air in the air hole. (b) The effect of different materials on the effective RI of the central core. (c) Effective RI of the x- and y-polarization modes. (d) Birefringence of the novel fiber with a side-hole. (e) The power ratio of the evanescent wave in the air hole of the fiber which filled in different materials. (f) The relationship between the wavelength and the RI of the center core in the side-hole and D-shape fiber.

second kind, respectively. The constants in Eqs. (8) shown at the bottom of this page, Should be determined by the continuous conditions for the tangential component at the boundaries. As a result, just like a conventional three-layered optical fiber, the propagation constants of the modes propagation in our fiber can also be calculated by solving the corresponding characteristic equation using these phase parameters [20].

This technique proves to be an effective and direct solution for optimizing structural fibers with lower errors compared to finite elements. Fig. 5(a) plots the effective RI of the fundamental mode at different d (where d is defined as $d = L\text{-}r_1\text{-}r_2$), it is worth noting that when $n_1 = 1$, the maximum difference is as small as 0.103×10^{-5} and 0.93×10^{-5} in $n_1 = 1.33$, so it is proved that this method is suitable for solving eccentric air hole microstructure fiber. A decrease in the difference of effective RI between finite element modeling (FEM) and conformal mapping method (CMM) is accompanied by an increase in the d distance of the eccentric air hole. When the position of the air hole deviates far enough, the effective RI value of the center core before and after the transformation is approximately equal.

The field distributions of the fundamental mode for $d = 4\ \mu$m on W-plane and G-plane is shown in Fig. 5(b). In the simulation, the parameters are measured by fiber samples, $n_1 = n_4$, $n_2 = 1.4555$, $n_3 = 1.458$ to evaluate the proposed method. Due to the presence of the air region, the distribution of the waveguide model in the central core is no longer a standard gaussian. However, after the conformal transformation of such a geometric structure, there is still a slight difference between the FEM and the analytical solution. In fact, the numerical results and analytical solutions are approximate, so they all have an error band. While, their difference is not enough to influence our comparative analysis. As can be seen from Fig. 5(b), there is not much difference between FEM and CMM, and the difference is so small that it can be ignored. Based on this data, it is proved that the proposed method is suitable for solving optical fibers with eccentric structure, and the accuracy of these two methods is proved.

C. Interaction Between Fluidic Materials and Evanescent Optical Field of the Center Core

Fig. 6(a) is the simulated field distribution, which can accurately describe the optical coupling between the two cores and the air hole. By using finite element software, the effective RI of the fiber mode at different wavelengths can be simulated. Fig. 6(b) reveals that due to the change in material type, the effective RI of the central core mode also changes at different wavelengths. Since the positions of the central core and the air

$$E_z = \begin{cases} AJ_m(u_1 r/R_2)\cos(m\varphi) & r < R_2 \\ [BI_m(u_2 r/R_2) + CK_m(u_2 r/R_2)]\cos(m\varphi) & R_2 < r < R_1 \\ DK_m(u_3 r/R_1)\cos(m\varphi) & r > R_1 \end{cases} \tag{8}$$

hole are almost tangent, the transform of the core will change sensitively with the vary of microfluid in the hole. We can find that as the RI of the material increases, the effective RI of the core also increases. Considering this microstructure fiber may have birefringence, we calculated the effective RI and birefringence of the central core in the x- and y-polarized as Fig. 6(c) and 6(d) shows. The birefringence parameter (*B*) of the fiber was calculated from the following expression

$$B = \left| Re\left(n^{x}_{eff}\right) - Re\left(n^{y}_{eff}\right) \right| \tag{9}$$

where n^{x}_{eff} and n^{y}_{eff} are the effective RI in the x- and y-polarized modes, respectively.

The evanescent field in the hole is considered to be able to evaluate the sensitivity of the sensor. In the case where different RI liquids were injected into the hole, the energy ratio between the hole and total at different wavelengths was analyzed. The energy ratio in the fiber is defined as $\eta = P_{\text{hole}}/P_{\text{total}}$ where P_{hole} represents the optical power in the hole, and P_{total} is the total power of the entire area. The power ratio between the air hole and the total region is shown in Fig. 6(e). The evanescent field in the air holes will increase as the microfluidic RI increases, and the optical wavelength increases. At the same time, we also compared with the RI sensitivity of D-shaped fiber with the same diameter and the distance with the cores. When the microflow $n = 1.45$, we have calculated the RI sensitivity and found that the difference between the side-hole fiber and the D-shaped fiber is infinitesimal, and the difference in RI sensitivity between them as low as 3×10^{-5}, D-shaped fiber is slightly higher than the side-hole fiber, is shown in Fig. 6(f).

As a result, the center core is significantly affected by the material in the air hole. However, the side core is not, because the distance between them is far enough so that they will not interfere with each other, so it has the potential to be an optical interference sensor. Furthermore, the characteristics of low consumption and high sensitivity are suitable as an interferential microstructure sensor. These advantages have attracted considerable attention in the use of optical fiber sensing.

This dual-core fiber can provide advantages such as size, trace sample measurement, material control in the air hole, and stable environment. Besides, there are some other superiorities, for example, the integrated optical path, and the analyzed signal is not affected by the electromagnetic field, and can be easily transmitted over long distances, and obtain clear results at low concentrations. The device combines material and light, and the light propagation path of the core will be affected by the microfluidic liquid RI. The optical signal can reflect certain characteristics of the detection material.

V. Conclusion

This paper presents a dual-core fiber with integrated microchannels. It has the inherent advantages of microchannel fiber, the length of the hole runs through the entire device and can hold a certain amount of material. This can reduce the experimental steps and sample dose. Especially, the structure of the central core is tangent to the edge of the air hole, when the analyte is a liquid, this will enable the core to directly interact with the sample. Through the interaction between the material in the microchannel and the evanescent lightwave field of the central nucleus, real-time monitoring and measurement of low concentration, liquid refractive index, and chemical substance absorption spectra can be realized. Besides, the dual-core fiber can integrate the optical interferometer into a single fiber. Therefore, the central core that interacts with the material can be used as a sensing arm, and the other arm can be used as a reference arm to achieve a highly integrated, highly sensitive optical fiber phase sensing system.

References

[1] P. S. J. Russell, “Photonic-crystal fibers,” *J. Lightw. Technol.*, vol. 24, no. 12, pp. 4729–4749, 2006.

[2] J. C. Knight, T. A. Birks, P. S. J. Russell, and J. P. de Sandro, “Properties of photonic crystal fiber and the effective index model,” *J. Opt. Soc. Amer. A*, vol. 15, no. 3, pp. 748–752, 1998.

[3] K. Saitoh and S. Matsuo, “Multicore fibers for large capacity transmission,” *Nanophotonics*, vol. 2, nos. 5/6, pp. 441–454, 2013.

[4] X. Zhang *et al.*, “In-fiber integrated optics: An emerging photonics integration technology [Invited],” *Chin. Opt. Lett.*, vol. 16, no. 11, 2018, Art. no. 110601.

[5] T. Hayashi, T. Taru, O. Shimakawa, T. Sasaki, and E. Sasaoka, “Design and fabrication of ultra-low crosstalk and low-loss multi-core fiber,” *Opt. Express*, vol. 19, no. 17, pp. 16576–16592, 2011.

[6] V. I. Kopp and A. Z. Genack, “Adding twist,” *Nature Photon.*, vol. 5, no. 8, pp. 470–472, 2011.

[7] V. I. Kopp, J. Park, M. Wlodawski, J. Singer, D. Neugroschl, and A. Z. Genack, “Chiral fibers: Microformed optical waveguides for polarization control, sensing, coupling, amplification, and switching,” *J. Lightw. Technol.*, vol. 32, no. 4, pp. 605–613, 2014.

[8] R. C. Qiu and I. T. Lu, “Guided waves in chiral optical fibers,” *J. Opt. Soc. Amer. A*, vol. 11, no. 12, pp. 3212–3219, 1994.

[9] S. Atakaramians, A. Argyros, S. C. Fleming, and B. T. Kuhlmey, “Hollow-core uniaxial metamaterial clad fibers with dispersive metamaterials,” *J. Opt. Soc. Amer. B*, vol. 30, no. 4, pp. 851–867, 2013.

[10] D. Pratap, S. A. Ramakrishna, J. G. Pollock, and A. K. Iyer, “Anisotropic metamaterial optical fibers,” *Opt. Express*, vol. 23, no. 7, pp. 9074–9085, 2015.

[11] D. K. C. Wu, B. T. Kuhlmey, and B. J. Eggleton, “Ultrasensitive photonic crystal fiber refractive index sensor,” *Opt. Lett.*, vol. 34, no. 3, pp. 322–324, 2009.

[12] K. S. Abedin *et al.*, “Amplification and noise properties of an erbium-doped multicore fiber amplifier,” *Opt. Express*, vol. 19, no. 17, pp. 16715–16721, 2011.

[13] O. A. Schmidt, T. G. Euser, and P. S. J. Russell, “Mode-based microparticle conveyor belt in air-filled hollow-core photonic crystal fiber,” *Opt. Express*, vol. 21, no. 24, pp. 29383–29391, 2013.

[14] P. Russell, “Photonic crystal fibers,” *Science*, vol. 299, no. 5605, pp. 358–362, 2003.

[15] C. E. Kerbage, B. J. Eggleton, P. S. Westbrook, and R. S. Windeler, “Experimental and scalar beam propagation analysis of an air-silica microstructure fiber,” *Opt. Express*, vol. 7, no. 3, pp. 113–122, 2000.

[16] H. Kober, *Dictionary of Conformal Representations*. New York, NY, USA: Dover, 1957.

[17] R. M. Morse and H. Feshbach, “Methods of theoretical physics,” *Amer. J. Phys.*, vol. 22, no. 12, pp. 5–12, 1953.

[18] C. Guan, L. Yuan, F. Tian, Q. Dai, and X. Tian, “Mode field analysis of eccentric optical fibers by conformal mapping,” in *Proc. 21st Int. Conf. Opt. Fibre Sensors (OFS21)). SPIE*, vol. 7753, 77535W, 2011.

[19] C. Y. H. Tsao, D. N. Payne, and L. Li, “Modal propagation characteristics of radially stratified and D-shaped metallic optical fibers,” *Appl. Opt.*, vol. 28, no. 3, pp. 588–594, Feb. 1989.

[20] C. Tsao, *Optical Fibre Waveguide Analysis*. Oxford, U.K.: Oxford Univ. Press, 1992.